# Three-Dimensional Quantitative Structure−Activity Relationships and Activity Predictions of Human TRPV1 Channel Antagonists: Comparative Molecular Field Analysis and Comparative Molecular Similarity Index Analysis of Cinnamides

Vellarkad N. Viswanadhan,*,† Yaxiong Sun,† and Mark H. Norman‡

*Molecular Structure and Design, and Medicinal Chemistry, Chemistry Research and Discovery, Amgen, Inc., One Amgen Center Drive, Thousand Oaks, California 91320-1789*

*Received March 8, 2007*

3D-QSAR models for human TRPV1 channel antagonists were developed based on comparative molecular field analysis (CoMFA) and comparative molecular similarity analysis (CoMSIA), using a training set of 61 cinnamide TRPV1 antagonists and tested on an independent test set of 47 antagonists. Molecular alignment procedure included weights for both internal energy and atom-to-atom matching against a reference or probe. Sensitivity of results on partial charge assignments was explored using multiple charge sets. AM1-BCC charge assignments gave better results for both CoMFA and CoMSIA models. For the best CoMFA model, the statistics are, $r^2 = 0.96$, $q^2 = 0.58$, $n = 61$ for the training set and $r^2 = 0.50$, $n = 47$ for the test set. For the best CoMSIA model, the statistics are $r^2 = 0.95$, $q^2 = 0.57$, $n = 61$ for the training set and $r^2 = 0.48$, $n = 47$ for the test set. These models are consistent with the proposed binding modes and interactions of known activators of the TRPV1 channel such as capsaicin, in a structural model of the TM3/4 helical region of TRPV1.

## Introduction

Transient receptor potential (TRP) superfamily of ion channels represent a class of polymodal, multifunctional cell sensors activated by a variety of gating stimuli that integrate multitudes of external or internal signals.[1] Hence, pathogeneses of several diseases and therefore the scope for therapeutic intervention can be understood by studies pertaining to these channels.[1−3] A notable member of the superfamily, TRPV1,[a] has been targeted in the treatment of pain and gastrointestinal disorders.[4−6] TRPV1 is activated by the vanilloid, capsaicin (the pungent component of chili peppers), and resiniferatoxin (RTX) from *Euphorbia resinifera*, as well as by endogenous activators (anandamide, OLDA, NADA, heat, and protons).[7] Based on the observations that rabbits are insensitive to capsaicin and lack detectable RTX binding in membranes prepared from their dorsal root ganglia, cloned rabbit TRPV1 (highly homologous to human and rat TRPV1) was used to identify key residues such as Tyr511, Leu/Met547, and Thr550 in transmembrane regions (transmembrane helices 3 and 4, TM3/4) of human TRPV1 that confer vanilloid selectivity.[3] These and additional observations such as the pharmacological differences of the agonists of rat and human TRPV1 were used to propose a model of the TM3/4 of rat and human TRPV1 bound to capsaicin or RTX.[3] As this model is hypothetical without experimental verification, there is a strong need to develop a three-dimensional quantitative structure−activity relationship (3D-QSAR) model to aid in the development of potent TRPV1 antagonists.[3] However, previous QSAR studies in this regard pertain only to capsaicin and related agonists.[8,9]

Recently, we identified a series of potent TRPV1 antagonists, structurally different from capsaicin and capsazepine.[10−12] This development gave us an opportunity to computationally model, rationalize, and predict the activities of TRPV1 antagonists. In the present report, we describe the development of 3D-QSAR models of cinnamide antagonists to facilitate further rational design of the TRPV1 antagonists. The present study uses comparative molecular field analysis (CoMFA)[13] and comparative molecular similarity index analysis (CoMSIA)[14] methodologies in an effort to gain insights into the steric, the electrostatic, and the hydrophobic interactions governing the activity of these cinnamides. Furthermore, consistency with the earlier proposed models[2,3] of the TM3/4 of rat and human TRPV1 bound to capsaicin is explored, and some conclusions are drawn with respect to the general nature of substitutions that enhance activity for the cinnamide chemotype.

## Methods

Molecular modeling tasks reported here were performed using FLAME[15] (*Fl*exibly *A*lign *Mol*ecules; employing MMFF forcefield[16] and GB/SA solvent model[17]), SYBYL 7.1,[18] and Gaussian98[19] software packages. All CoMFA[13] and CoMSIA[14] calculations were performed using SYBYL 7.1.[18]

**Molecular Database, Reference Molecule, and Reference Conformation.** Earlier publications described the synthesis and the structure−activity relationships of the cinnamide antagonists of TRPV1 and their conformationally restricted analogs.[11,12] A set of 61 molecules belonging to the cinnamide series were considered as the training set for the present analysis. One of the first potent molecules identified from internal screening efforts,[20] a cinnamide, shown in Figure 1a, **1** (AMG9810),[11,12] with an $IC_{50}$ of 0.023 $\mu$M, is taken as the reference. Compound **1** blocks the TRPV1 activation induced with capsaicin (acid (pH 5), heat (45 °C)), and the endogenous activators of TRPV1 such as anandamide.[20]

The molecular modeling study of **1** was carried out using molecular dynamics/mechanics and ab initio quantum mechanics. A conformational search was carried out using high-temperature molecular dynamics. Simulations were conducted using the program, FLAME,[15] which employs the MMFF forcefield[16] and the

* To whom correspondence should be addressed. Amgen, Inc., One Amgen Center Drive, MS 29-M-B, Thousand Oaks, California 91320. Tel.: 805-447-1327. Fax: 805-480-3015. E-mail: visv@amgen.com.

† Molecular Structure and Design.

‡ Medicinal Chemistry.

[a] Abbreviations: TRPV1, transient receptor potential vanilloid 1; TM3/4, transmembrane helices 3 and 4; AM1-BCC, Austin Model 1−bond charge correction; MMFF, Merck molecular force field; GB/SA, generalized Born/solvent accessibility; FLAME, flexibly align molecules.

10.1021/jm070261k CCC: $37.00 
Published on Web 10/19/2007

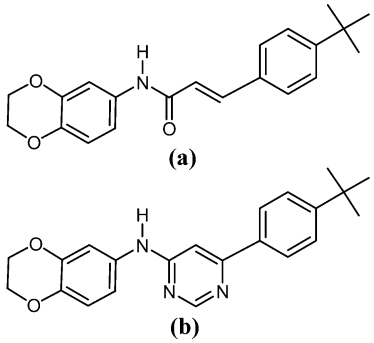

**Figure 1.** (a) Cinnamide **1**, and (b) **1A**, the conformationally restricted analog of **1**.

GB/SA solvent model[17] in the aqueous medium. The low-energy conformations of the reference compound were chosen for further optimization by ab initio quantum mechanics. Quantum mechanical calculations were performed using the density functional theory, as implemented in Gaussian98[19] software, utilizing the B3LYP hybrid density functional and the 6-31G* basis set.

Figure 2 shows a conformationally restricted analog, **1A** ($IC_{50}$ = 0.051 $\mu$M) of the reference cinnamide. Using the ab initio calculated lowest energy conformations of the reference as templates, **1A** was aligned on these templates and the alignments were compared. Additionally, a molecular mechanics-based flexible alignment of **1** and **1A** was performed using the "flexboth" option of FLAME.[15] The bioactive conformation of cinnamides (the reference conformation) was assessed and arrived at based on these calculations.

Tables 1−6 lists the molecules used in this study along with their biological activities (with $IC_{50}$ values in molar units) on logarithmic scale, $pIC_{50} = -\log(IC_{50})$. Reported biological activities[11] were obtained by employing rat−human chimera of the TRPV1 channel, recombinantly expressed in Chinese hamster ovary (CHO) cells. The compounds explored include the substitutions to the phenyl (Table 1), the substitutions to the acryl amide core (Table 2), the substitutions to the aniline part (Table 3), replacements to the phenyl (Table 4), the replacements to the benzodioxane and the phenyl groups (Table 5), and the replacements to the acrylamide core (Table 6). An independent set of 47 molecules was selected as the test set, which belongs to the same family of cinnamides but contains several compounds with significantly different substituents relative to those in the training set. These compounds and their activities (on logarithmic scale, $pIC_{50}$) are shown in Table 7.

**Alignment of the Molecules in the Training and the Test Sets.** The molecules shown in the Tables 1−7 were generated using CONCORD,[21,22] version 4.08. The assessed bioactive conformation of **1** (the reference conformation) was used as the template for the alignment of all the molecules considered. Molecules in the training set were aligned using a recently developed alignment method, FLAME[15]. FLAME uses an alignment procedure that performs a simultaneous optimization of internal energies and the alignment score of two or more molecules. In this procedure, first, the initial alignments are generated using a genetic algorithm to optimize maximum common pharmacophores. Second, a simultaneous optimization of internal energies and the alignment score is carried out using a scoring function that balances internal energies of probe ($U_P$) and target ($U_T$) molecules and alignment. The functional form for this scoring function is given in eq 1 where $F$ is the score, $U_P$ is the internal energy of the probe molecule, $U_T$ is the internal energy of the target molecule, $A$ is the alignment score for each alignment and includes individual contributions from all probe and target atoms to the alignment in terms of chemical matching weight, probe weight, and target pharmacophore weight, and $T$ refers to "temperature factor", a term used to control relative weights of internal energies and the alignment.

$$F = U_P + U_T - TA \quad (1)$$

**Table 1.** First Set of Compounds in the Training Set; the Chemotype and Specific Substitutions are Identified[a]

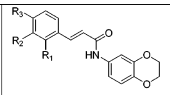

| Compound no. | $R_1$ | $R_2$ | $R_3$ | $pIC_{50}$ (expt.) | $pIC_{50}$ (calc.) |
|---|---|---|---|---|---|
| 1 | | |  | 7.59 | 6.65 |
| 2 | | |  | 6.23 | 4.90 |
| 3 | | |  | 6.47 | 6.51 |
| 4 | | | | 5.29 | 6.43 |
| 5 | | |  | 6.67 | 6.24 |
| 6 | | |  | 5.83 | 6.12 |
| 7 | | |  | 4.40 | 6.31 |
| 8 | | |  | 6.92 | 7.02 |
| 9 | | |  | 5.73 | 4.94 |
| 10 | | |  | 4.40 | 5.32 |
| 11 | | |  | 6.53 | 6.46 |
| 12 | | |  | 5.99 | 6.09 |
| 13 | | |  | 7.01 | 6.86 |
| 14 | | |  | 6.51 | 6.58 |
| 15 | | |  | 6.61 | 6.10 |
| 16 | |  | | 6.26 | 5.68 |
| 17 |  | |  | 6.80 | 6.93 |
| 18 | 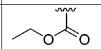 | |  | 7.58 | 7.58 |

[a] All the calculated values reported in Tables 1−7 ($pIC_{50}$s) are based on Model 3 (based on $IC_{50}$ values in molar units).

Only the query (or target) compound was subjected to optimization. Thus, all molecules in the training and the test databases were subjected to pairwise alignment, with the reference conformation of **1** as the probe and each of the other molecules being the query (or target) molecule in turn. This scoring/optimization procedure is applied to the entire GA-optimized population of the aligned target structures, and the resulting alignment scores are sorted and the best scored alignment of the query molecule is saved for developing the 3D-QSAR models.

**Comparative Molecular Field Analysis and Comparative Molecular Similarity Analysis.** SYBYL 7.1[18] was used to generate the CoMFA[13] steric and electrostatic fields, using the L-J and the Coulombic potentials, respectively. The electrostatic fields were computed using two different charge calculation methods (Gasteiger−Huckel,[18,23] AM1-BCC[24]) to explore the sensitivity of the charge calculation method on the final results. Apart from this, the standard parameters implemented in SYBYL 7.1[18] were used. An $sp^3$-hybridized carbon probe atom with a charge of +1.0 was used for the calculation of the steric and the electrostatic fields of CoMFA. The standard grid spacing[18] (of 2 Å) is used for all the models described here.

**Table 2.** Second Set of Compounds in the Training Set; the Chemotype and Specific Substitutions are Identified

| | 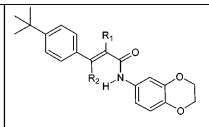 | | | |
|---|---|---|---|---|
| Compound no. | $R_1$ | $R_2$ | $pIC_{50}$ (expt.) | $pIC_{50}$ (calc.) |
| 19 |  | | 6.30 | 6.11 |
| 20 |  | | 6.78 | 6.27 |
| 21 | |  | 7.09 | 7.11 |
| 22 | | 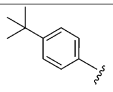 | 5.60 | 7.16 |
| 23 | |  | 7.32 | 6.83 |
| 24 | | 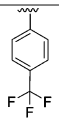 | 7.33 | 7.28 |
| 25 | |  | 7.69 | 7.19 |
| 26 | |  | 7.38 | 7.46 |
| 27 | |  | 6.84 | 7.06 |
| 28 | |  | 6.92 | 6.66 |
| 29 | |  | 7.25 | 7.09 |
| 30 |  | | 4.97 | 6.19 |

**Table 3.** Third Set of Compounds in the Training Set; the Chemotype and Specific Substitutions are Identified

| | 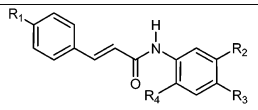 | | | | | |
|---|---|---|---|---|---|---|
| Compound no. | $R_1$ | $R_2$ | $R_3$ | $R_4$ | $pIC_{50}$ (expt.) | $pIC_{50}$ (calc.) |
| 31 |  | | | | 6.57 | 6.97 |
| 32 |  |  | | | 6.64 | 7.55 |
| 33 |  |  | | | 7.24 | 6.91 |
| 34 |  | |  | | 6.78 | 6.62 |
| 35 |  |  | | | 0.99 | 6.99 |
| 36 |  |  | | | 0.76 | 6.76 |
| 37 |  |  | | | 2.39 | 8.39 |
| 38 |  |  | | | 1.74 | 7.74 |
| 39 |  |  | | | 1.73 | 7.73 |
| 40 |  | 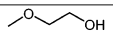 | | | 6.07 | 7.53 |
| 41 |  |  | | | 0.41 | 6.41 |
| 42 |  |  | | | 2.44 | 8.44 |
| 43 |  |  | | | 1.59 | 7.59 |
| 44 |  |  | | | 1.26 | 7.26 |
| 45 |  | | |  | 6.07 | 6.51 |
| 46 |  |  | | | 7.48 | 7.68 |
| 47 |  |  | | | 6.00 | 5.59 |

The CoMSIA[14] fields (the steric, the electrostatic, and the hydrophobic) were generated using the standard parameters implemented in SYBYL.[18] The CoMSIA electrostatic fields were also calculated using the Gasteiger−Huckel[18,23] and the AM1-BCC[24] charge sets, separately. The standard probe for CoMSIA has a unit charge, a 1 Å radius, and a unit hydrophobicity value. The CoMSIA hydrophobicity fields were calculated using the atomic hydrophobicity constants given by Viswanadhan et al.[25] for the ALOGP atom types.

For developing the CoMFA and the CoMSIA models from the corresponding fields, a partial least-squares (PLS) analysis was carried out as implemented in SYBYL 7.1.[18] A LOO (Leave-One-Out) cross-validation procedure was used to check the statistical significance of results. The SAMPLS[26] method enabled quick determination of the optimal number of components. After this, a final noncross-validated model was developed and used for the predictions on an independent test set of 47 molecules identified in the Table 7.

## Results and Discussion

**Assessment of the Bioactive (Reference) Conformation.** Compound **1** (Figure 1a) was used as the reference molecule. As the structure of TRPV1 receptor is unknown, the reference (or the bioactive) conformation was deduced, based on (i) a conformational analysis of the reference molecule and (ii) a flexible alignment of the reference with a conformationally restricted potent analog, **1A** (Figure 1b). As described in the methods, FLAME[15] was used to perform a conformational analysis of **1** and this was followed by an ab initio quantum mechanics optimization of the lowest-energy conformations, performed for each conformer at B3LYP/6-31G* level, as implemented in the Gaussian98[19] program package. This calculation led to the identification of the *s-cis*-conformer of the cinnamide moiety as the lowest-energy conformation, which is lower in energy by 2.6 kcal/mol relative to the *s-trans*-conformer.[12] Using the *s-cis*- and *s-trans*-conformations of **1** as independent templates, **1A** (which has a 4-amino pyrimidine core, replacing the acrylamide moiety) was aligned on each template and the two alignments were compared. It was seen

**Table 4.** Fourth Set of Compounds in the Training Set; the Chemotype and Specific Substitutions are Identified

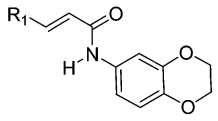

| Compound No. | $R_1$ | $pIC_{50}$ (expt.) | $pIC_{50}$ (calc.) |
|---|---|---|---|
| 48 | 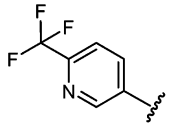 | 5.97 | 5.75 |
| 49 | 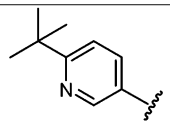 | 6.74 | 6.98 |
| 50 | 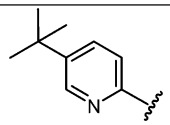 | 5.97 | 6.74 |
| 51 | 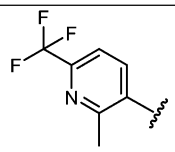 | 5.95 | 6.49 |

**Table 5.** Fifth Set of Compounds in the Training Set; the Chemotype and Specific Substitutions are Identified

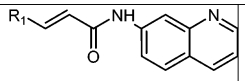

| Compound No. | $R_1$ | $pIC_{50}$ (expt.) | $pIC_{50}$ (calc.) |
|---|---|---|---|
| 52 | 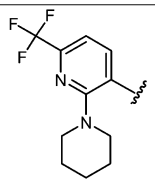 | 8.94 | 8.64 |
| 53 | 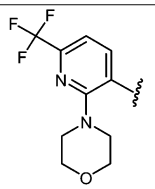 | 8.78 | 8.75 |

that the *s-cis*-conformation of **1** aligns much better with **1A**, relative to the higher-energy conformation, *s-trans*. Not surprisingly, a flexible alignment of **1** and **1A** using FLAME[15] (with "flexboth" option which allows torsional flexibility for both molecules) also led to the identification of the *s-cis*-conformation of **1**, which is then taken as the bioactive or reference conformation. The suitability of the 4-amino pyrimidine as a core replacement to the cinnamide series and the corresponding SAR described earlier[12] offers strong additional support to the deduction that the global minimum energy conformation of **1** (*s-cis*) is the bioactive or reference conformation.

**Table 6.** Sixth Set of Compounds in the Training Set; the Chemotype and Specific Substitutions are Identified

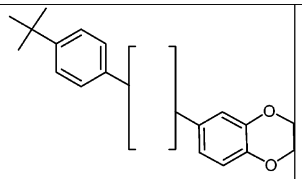

| Compound no. | Spacer unit | $pIC_{50}$ (expt.) | $pIC_{50}$ (calc.) |
|---|---|---|---|
| 54 | 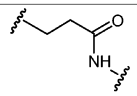 | 6.65 | 6.45 |
| 55 | 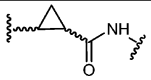 | 5.44 | 6.34 |
| 56 | 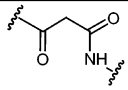 | 6.23 | 5.86 |
| 57 | 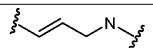 | 4.40 | 5.02 |
| 58 | 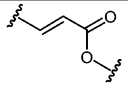 | 6.06 | 5.23 |
| 59 | 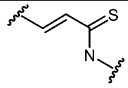 | 6.41 | 6.55 |
| 60 | 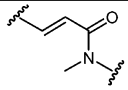 | 4.71 | 6.04 |
| 61 | 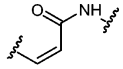 | 5.72 | 5.36 |

**Alignment of Molecules in the Training and Test Sets.** Alignment of all the analogs by FLAME[15] followed an automated procedure (described in the Methods). Equal weights were assigned for the internal energy (based on MMFF)[16] and the alignment scores. As the molecules described in the present study belong to the same family of cinnamides, aligned molecules were all at (or relatively close to) the global minimum energy (*s-cis*) conformation. Figure 2 shows an alignment of some representative molecules in the training set.

**CoMFA 3DQSAR Models.** Using CoMFA[13] default parameters for the training set, predictive 3D-QSAR models were obtained, as determined by cross validation. An optimal number of components for each cross validated model (based on $q^2$) was determined using the SAMPLS method.[26] Gasteiger−Huckel[18,23] and AM1-BCC[24] partial charge sets were used to develop the CoMFA models. The use of *region focusing*[27] (as implemented in SYBYL 7.1[18]) improved the models. Cross-validated $R^2$-guided region selection[27] ($Q^2$-GRS) or *region focusing*[27] optimizes the CoMFA/CoMSIA models by (i) subdividing the rectangular lattice (obtained initially with conventional CoMFA/CoMSIA models) into a number of smaller boxes, (ii) performing independent analyses for these boxes to decipher the regions which contribute significantly to the model, and (iii) combining these regions, resulting in a better model, eliminating noise. The results are shown in the Table 8. It can be seen from the Table 8 that the AM1-BCC[24] charge

**Table 7.** Set of Compounds in the Test Set; the Chemotype and Specific Substitutions are Identified

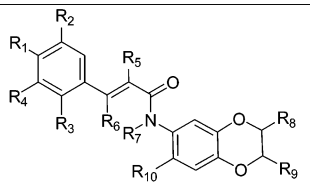


| Compound no. | $R_1$ | $R_2$ | $R_3$ | $R_4$ | $R_5$ |
|---|---|---|---|---|---|
| 62 |  | | | | |
| 63 |  | | | |  |
| 64 |  | |  | | |
| 65 |  | | | |  |
| 66 |  |  | |  | |
| 67 |  | | | | |
| 68 | |  | | | |
| 69 |  |  | | | |
| 70 |  |  | | | |
| 71 | |  | | | |
| 72 | | |  | | |
| 73 |  | |  | | |
| 74 |  | | | | |
| 75 |  | | | | |
| 76 |  | | | | |
| 77 | |  | | | |
| 78 |  | | | | |
| 79 |  | | | | |
| 80 | |  | | | |
| 81 |  | | | | |
| 82 |  | | | | |
| 83 |  |  | | | |

| Compound no. | $R_1$ | $R_2$ | $R_3$ | $R_4$ | $R_5$ |
|---|---|---|---|---|---|
| 84 |  | | | | |
| 85 |  |  | | | |
| 86 |  | | | | |
| 87 |  | | | | |
| 88 |  | | | | |
| 89 |  | | | | |
| 90 | | | |  | |
| 91 |  | | | | |
| 92 |  | | | | |
| 93 | | |  | | |
| 94 |  | | | | |
| 95 |  | | | | |
| 96 |  | | | | |
| 97 | |  | | | |
| 98 | |  | | | |
| 99 |  | | | | |
| 100 | | |  | | |
| 101 |  | | | | |
| 102 |  | |  | | |
| 103 |  | | | | |
| 104 |  | | | | |
| 105 |  | | | | |
| 106 |  | | | | |
| 107 |  | | | | |
| 108 |  | |  | | |

**Table 7.** Continued

| $R_6$ | $R_7$ | $R_8$ | $R_9$ | $R_{10}$ | pIC50 (expt.) | pIC50 (pred.) |
|---|---|---|---|---|---|---|
|  | | | | | 6.92 | 7.09 |
| | | | | | 4.81 | 5.50 |
| | | | | | 8.21 | 7.69 |
| | | | | | 6.26 | 5.85 |
| | | | | | 4.40 | 5.16 |
| | | | | | 5.88 | 5.70 |
| | | | | | 6.39 | 6.18 |
| | | | | | 6.35 | 6.44 |
| | | | | | 5.88 | 6.15 |
| | | | | | 5.92 | 6.70 |
| | | | | | 6.19 | 5.33 |
| | | | | | 5.44 | 6.02 |
| | | | | | 6.13 | 5.42 |
| | | | | | 4.40 | 4.67 |
| | | | | | 5.63 | 6.31 |
| | | | | | 5.38 | 5.60 |
| 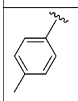 | | | | | 6.61 | 6.20 |
| | | | | | 6.29 | 6.68 |
| | | | | | 5.79 | 6.11 |
| | | | | | 7.32 | 6.06 |
| | | | | | 6.38 | 6.60 |
| | | | | | 6.34 | 6.16 |
| | | | | | 5.45 | 5.52 |
| | | | | | 6.89 | 7.15 |
| 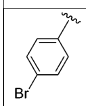 | | | | | 7.22 | 7.21 |
| 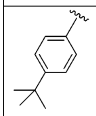 | | | | | 7.03 | 6.46 |
| 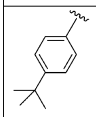 | | | | | 7.37 | 7.11 |
| 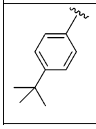 | | | | | 7.41 | 7.01 |

| $R_6$ | $R_7$ | $R_8$ | $R_9$ | $R_{10}$ | pIC50 (expt.) | pIC50 (pred.) |
|---|---|---|---|---|---|---|
| 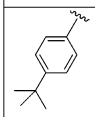 | | | | | 7.23 | 6.70 |
| | | | | | 6.87 | 6.18 |
| | | | | | 6.26 | 6.27 |
| 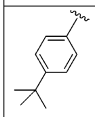 | | | | | 6.55 | 6.94 |
|  | | | | | 6.46 | 7.12 |
| | |  | | | 6.59 | 6.56 |
| | |  | | | 6.66 | 6.78 |
| 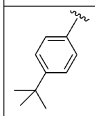 | | | | | 6.81 | 6.63 |
| 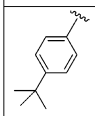 | | | | | 6.48 | 6.59 |
| | | |  | | 7.62 | 6.38 |
| 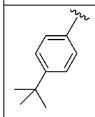 | | | | | 6.82 | 7.22 |
| 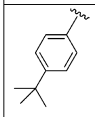 | | | | | 7.34 | 6.09 |
| | | | | | 6.35 | 7.75 |
| | | |  | | 6.18 | 6.09 |
| | | |  | | 5.99 | 6.09 |
| | | | 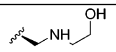 | | 6.16 | 6.31 |
| | | | 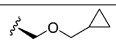 | | 6.48 | 6.16 |
| | | |  | | 5.90 | 6.17 |
| | | | | | 6.34 | 7.25 |

set gives better statistical results ($q^2$ and $r^2$ for the training set and $r^2$ for the independent test set) than the Gasteiger−Huckel charge set.

Figure 3a,b shows the CoMFA steric and electrostatic fields overlaid some representative compounds. In Figure 3a, the green and the yellow contours represent sterically attractive and repulsive regions, respectively. The large alkyl groups such as the *t*-butyl are preferred at the *para*-position of the phenyl ring, while even larger groups such as the phenyl are not preferred due to the overlap with the repulsive region (the small yellow contour). Two other prominent repulsive regions include the region close to the central acryl amide moiety and another at the 2,3-dihydro[1,4]benzo-dioxine ring. Figure 3b shows CoMFA electrostatic fields, with blue contours representing preference for electropositive and red contours representing preference for electronegative atoms/groups. Two prominent red regions show the significance of carbonyl of the amide and electronegative groups (e.g., $CF_3$) attached to the *para*-position of the phenyl.

**CoMSIA 3D QSAR Models.** CoMSIA,[14] a newer 3D-QSAR technique, allows more incisive dissection of different binding affinity contributions, including the steric and electrostatic contributions as well as the entropic effects, which are harder to quantify. For modeling this contribution, CoMSIA integrates an empirical field based on a set of atomic hydrophobicity constants into a formalism similar to CoMFA type

**Figure 2.** Alignment of some molecules in the training set. Compounds shown are **1** (light brown), **3** (pink), **7** (dark green), **9** (light gray), **17** (yellow), **19** (light green), **22** (orange), **32** (white), **33** (cyan), **45** (blue), and **53** (purple).

**Table 8.** Statistics of CoMFA Models for the Training and Test Sets

| | CoMFA | | |
|---|---|---|---|
| parameter | model 1[a] | model 2[b] | model 3[c] |
| | Training Set | | |
| $r^2$ | 0.95 | 0.93 | 0.96 |
| SEE | 0.23 | 0.28 | 0.22 |
| fraction: | | | |
| steric | 0.47 | 0.45 | 0.46 |
| electrostatic | 0.53 | 0.55 | 0.54 |
| $q^2$ | 0.49 | 0.48 | 0.58 |
| No. of components (opt) | 8 | 5 | 8 |
| No. of compounds | 61 | 61 | 61 |
| | Test Set | | |
| $r^2$ | 0.25 | 0.45 | 0.50 |
| SD of residuals | 0.72 | 0.57 | 0.57 |
| *p* value | 0.0003 | <0.0001 | <0.0001 |
| No. of compounds | 47 | 47 | 47 |

[a] Results with two fields and Gasteiger-Huckel[18,23] charges. [b] Results with two fields and AM1-BCC[24] charges. [c] Results with two fields and AM1-BCC[24] charges, *region focusing*[27] included.

analyses. An important feature of this formalism is the use of a Gaussian function to probe the similarity of each molecule with respect to a probe atom scanning a lattice embedding all aligned molecules, with no cutoffs for inside and outside of a molecule.

Table 9 shows the statistics of CoMSIA models for the training and the test sets. Comparison of the results of model 1 with those of models 2 and 3 shows that models using the AM1-BCC[24] charge sets give better results compared to those using the Gasteiger−Huckel charges. A slightly better $q^2$ was obtained when *region focusing* is included (model 3) for the training set. Tables 1−7 show the training and the test set data ($pIC_{50}$s, observed and predicted, based on the CoMSIA model with *region focusing* included), respectively. A strong influence of the AM1-BCC[24] charge sets in obtaining better results is clearly seen for the test set. However, *region focusing* does not appear to have much influence on the test set results. Figure 4a−c shows isopotential contours elucidating (a) the steric, (b) the electrostatic, and (c) the hydrophobicity CoMSIA fields, respectively. Figure 4a shows sterically favored (green) and disfavored (yellow) regions. The two prominent green regions show that steric bulk in these regions contributes to binding affinity (as in the case of **24**), whereas a prominent disfavored region (shown in yellow) indicates a loss in binding affinity when that region is occupied (as in the case of **22**). The significance of an amide group is highlighted in Figure 4b by the cyan and the red contours, which favor the electropositive and the electronegative groups, respectively. Several compounds

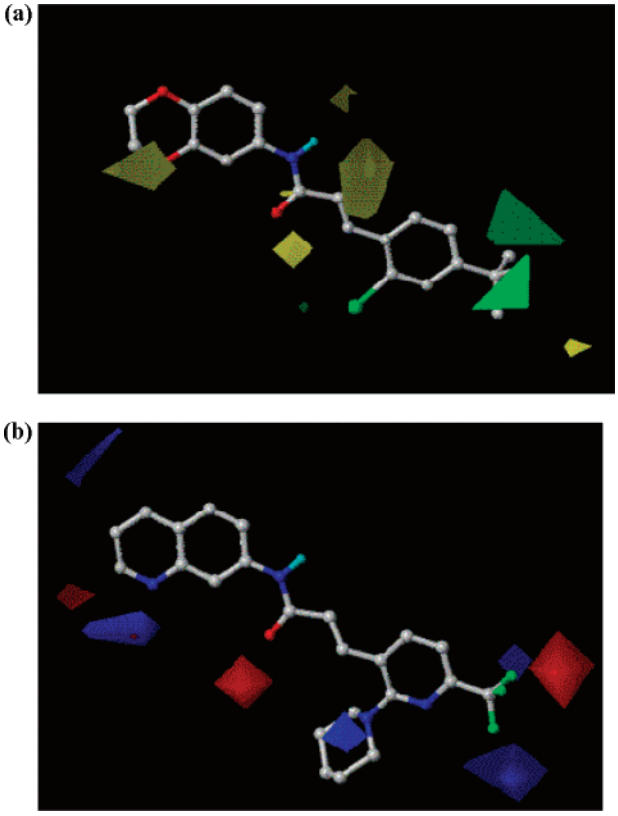


**Figure 3.** (a) CoMFA steric fields overlaid on **17** (color code: favored, green; disfavored, yellow). (b) CoMFA electrostatic fields overlaid on **52** (color code: increase in positive charge favored, blue; increase in negative charge favored, red).

**Table 9.** Statistics of CoMSIA Models for the Training and Test Sets

| | CoMSIA | | |
|---|---|---|---|
| parameter | model 1[a] | model 2[b] | model 3[c] |
| | Training Set | | |
| $r^2$ | 0.88 | 0.94 | 0.95 |
| SEE | 0.36 | 0.25 | 0.24 |
| fraction: | | | |
| steric | 0.18 | 0.16 | 0.21 |
| electrostatic | 0.45 | 0.48 | 0.45 |
| hydrophobic | 0.37 | 0.36 | 0.34 |
| $q^2$ | 0.49 | 0.52 | 0.57 |
| No. of components (opt) | 5 | 7 | 8 |
| No. of compounds | 61 | 61 | 61 |
| | Test Set | | |
| $r^2$ | 0.24 | 0.51 | 0.48 |
| SD of residuals | 0.67 | 0.45 | 0.47 |
| *p* value | 0.0005 | <0.0001 | <0.0001 |
| No. of compounds | 47 | 47 | 47 |

[a] Results with three fields and Gasteiger−Huckel[18,23] charges. [b] Results with three fields and AM1-BCC[24] charges. [c] Results with three fields and AM1-BCC[24] charges, *region focusing*[27] included.

(**57**−**60**, see Table 6) lacking this amide show some loss of potency. In the case of **61**, because of the configuration of the cinnamide, the molecule does not align well with **1** and loses activity. The hydrophobic field contours (Figure 4c) identify the favored (pink) and the disfavored (gray) regions overlaid on **17**. These hydrophobicity contours are also helpful in rationalizing the activity of several compounds. Compound **4**, for example, lacks the hydrophobic substituents at the phenyl (a pink region in Figure 4c), causing a loss of activity. Compound **18**, with a bigger hydrophobic group at $R_1$ (favored, at a pink region), is more potent relative to **17**. Contrasting

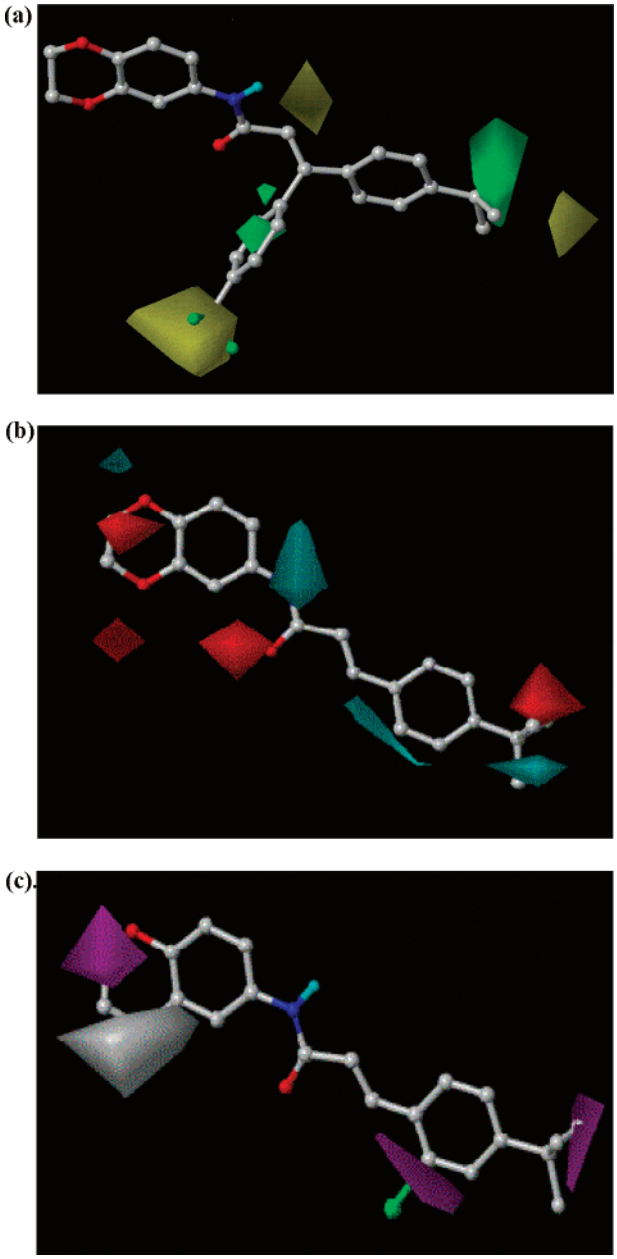


**Figure 4.** (a) CoMSIA steric fields overlaid on **24** (color code: favored, green; disfavored, yellow). (b) CoMSIA electrostatic fields overlaid on **1** (color code: increase in positive charge favored, blue; increase in negative charge favored, red). (c) CoMSIA hydrophobic fields overlaid on **17** (color code: favored, pink; disfavored, gray).

**63** and **64** (in the test set) provides an example of how the 3D-QSAR models may be used prospectively. These compounds differ from **1** (the reference) by the presence of an additional cyclopentyl group at the $R_5$ (**63**) or $R_3$ (**64**) position (Table 7). Contours shown in Figure 4c correctly identify the position ($R_3$) appropriate for a hydrophobic substitution and in these cases, the predictions agree well with the experimental results.

**Comparison of the CoMSIA and CoMFA Field Maps and the Results.** As the CoMFA[13] and CoMSIA[14] models are basically different ways of creating and comparatively representing the interaction fields around the ligands, it should be interesting to compare and contrast the two types of field contours in light of the activity data. Unlike CoMFA,[13] the hydrophobic and steric fields are differentiated by CoMSIA,[14] and this aspect was helpful in identifying the precise nature of substituents (polar or nonpolar) that can improve activity. On the other hand, the CoMFA fields are fewer and simpler to analyze.

The yellow region near one of the oxygens of dihydro[1,4]-dioxine ring in CoMFA steric field map (Figure 3a) corresponds to the gray region in the CoMSIA hydrophobic field map at that ring (Figure 4c). These regions indicate unfavorable interactions when that region is accessed with hydrophobic atoms (e.g., **32**, **34**, or **35**). Activities for other related compounds (see Table 3), such as **38**, can be understood by considering both the electrostatic and hydrophobic CoMSIA contours. In that region (of dihydro[1,4]dioxine ring), the CoMSIA field contours show two electronegative or red regions, one electropositive or blue region (Figure 4b), as well as pink (favorable) and gray (unfavorable) regions (Figure 4c) relating to hydrophobicity. Thus, for these regions, the CoMSIA contours offered more useful detail than CoMFA contours.

Understandably, the electrostatic field maps (Figure 3b and Figure 4b) of CoMSIA[14] and CoMFA[13] have similar characteristics, as both methods are based on the AM1-BCC[24] charge sets. Both do identify the region close to the amide carbonyl (shown in red) as favoring the electronegative atoms on the ligands (this explains why **59** is much less active relative to **1**). The electropositive and the electronegative regions on the lower right (common to CoMSIA and CoMFA) arise from differences in charge distributions of compounds in the training set, as this region is generally occupied halogens, small polar groups such as methoxy and hydroxyl, or small hydrophobic groups such as the chloro, the trifluoro methyl, or the *t*-butyl groups in the training set. At the bottom of the fused ring on the top left, one may see some red and blue regions in CoMFA electrostatic maps but not in the corresponding CoMSIA maps. The CoMFA model interprets the activity of **46**, **38**, and **42** as arising from the electrostatic interactions of the endocyclic amide group with the receptor. In the case of the CoMSIA model, this region is occupied by a gray contour, which represents an unfavorable hydrophobic interaction (i.e., favorable to polar interactions) consistent with the CoMFA model.

The CoMFA steric fields contain the characteristics of both the hydrophobic and the steric fields of CoMSIA. For **17**, Figure 4c shows the CoMSIA hydrophobic field map, whereas Figure 3a shows the CoMFA steric map. The CoMFA steric maps (Figure 3a) show sterically attractive regions (in green) at the *para*-position of the phenyl ring on the right-hand side. These regions are also captured by the CoMSIA hydrophobic field (Figure 4c). However, CoMSIA makes a distinction between the hydrophobic and the hydrophilic substituents and this helps rationalize the loss of activity when the polar (or the partly polar) groups are placed in these regions (e.g., **8**, **9**, and **10** relative to **1**).

A repulsive region to the right of the *para*-substituted phenyl is seen in both the CoMSIA and the CoMFA steric maps and this accounts for the loss of activity when a larger substituent such as phenyl is added at the *para*-position of the ring (e.g., **7**). The steric field maps of both CoMFA and CoMSIA capture the loss of activity when the amide NH is capped (**60**), as indicated by the small yellow (repulsive) region close to the amide proton in CoMFA and CoMSIA steric maps. CoMSIA additionally captures two attractive regions in the hydrophobic field maps, which are not reflected in the CoMFA maps. The magenta-colored region at the top left of dihydro[1,4]dioxine ring indicates the importance of occupying that region with relatively more hydrophobic atoms (consider **41** which has an amide in that region, and is less active). Thus, these CoMSIA

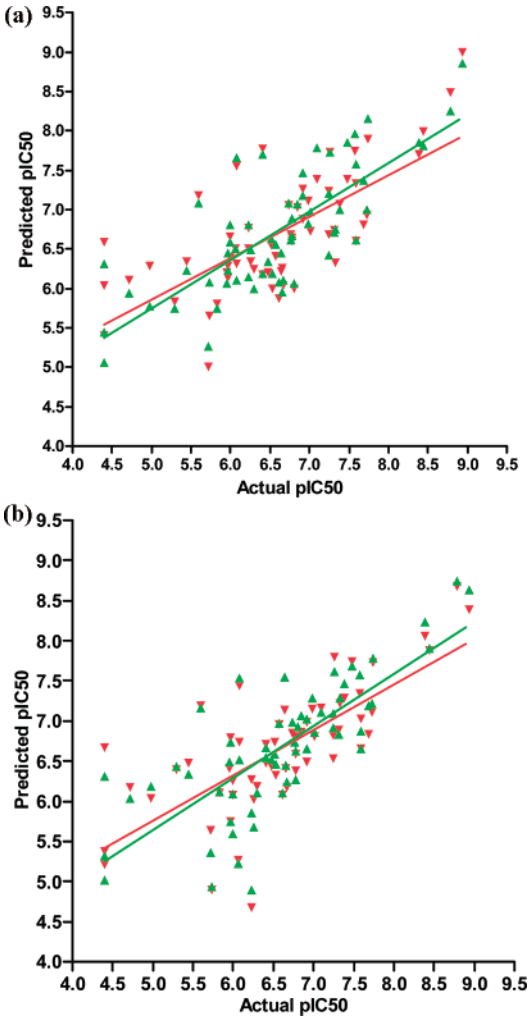


**Figure 5.** (a) Results of the cross-validation runs. The red triangles represent CoMFA results with AM1-BCC[24] charges, and green triangles represent CoMFA results with *region focusing included*.[27] (b) Results of the cross-validation runs. The red triangles represent the CoMSIA results with AM1-BCC charges, and green triangles represent CoMSIA results with *region focusing*[27] included.

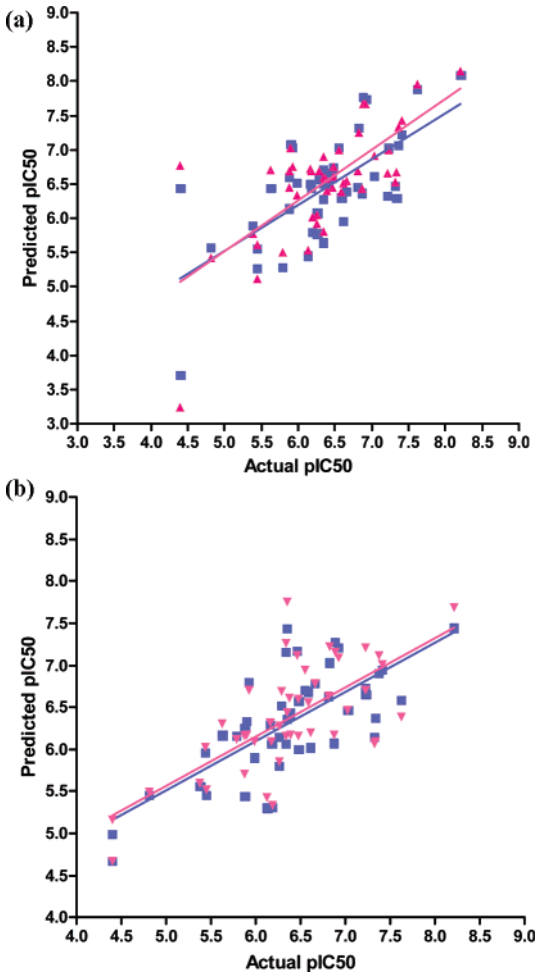


**Figure 6.** (a) Test set results based on the CoMFA analyses. The blue squares represent the CoMFA results with the AM1-BCC[24] charges and the red triangles represent the CoMFA results with the AM1-BCC[24] charges and include *Region Focusing*. (b) Test set results based on CoMSIA analyses. The blue squares represent the CoMSIA results with AM1-BCC[24] charges and the red triangles represent the results with AM1-BCC[24] charges and include *region focusing*[27].

contours offered additional insights into the nature of the groups contributing to activity.

As shown in Tables 8 and 9, CoMFA and CoMSIA gave similar results for both the training and the test sets, with some improvement when *region focusing*[27] is included in the models (model 3), particularly for CoMFA. Tables 1−6 list the CoMSIA predictions (from the cross validation runs of the model 3) along with the observed activities. Table 7 also lists the CoMSIA predicted values for the test set (molecules not included in the training set). Figure 5a,b shows the scatter plots of CoMFA predictions and Figure 6a,b shows the scatter plots of CoMSIA predictions. In both cases, the results from the models 2 and 3 are shown in different colors, along with the fitted lines. The model 3 (with *region focusing*[27]) predictions do not appear to be better in all cases, though they are arguably closer to the fitted line for more active compounds. The scatter plots for the CoMFA models indicate that molecules that are less active are less accurately predicted.

**Sensitivity of Results to the Choice of Methodology and Charge Models.** The methodology of 3D-QSAR models and the treatment of electrostatics are two aspects that deserve a careful consideration in developing a predictive model. Though the use of semiempirical charge sets is common in 3D-QSAR literature[13,14,28] as a better treatment of electrostatics relative to the Gasteiger−Marsili[23] (or Gasteiger−Huckel[18,23]) charge sets, they are "population" quantities based on the occupancies of atomic orbitals and are not meant to reproduce electrostatic potentials (ESPs) of the molecule, an obviously better choice in modeling receptor interactions or quantitative comparison of molecules as in 3D-QSAR.[28] However, the older HF/6-31G* ESP-derived charges could be "unstable", that is, can exhibit considerable variation for similar functional groups resulting in exaggerated differences in assigned partial charges.[29] Hence, HF/6-31G* RESP-derived charges are more appropriate for molecular simulations.[29] Jakalian et al.[24] developed a quick and efficient method (AM1-BCC) based on AM1 semiempirical charge calculation and parameterized bond charge corrections (BCCs). As AM1-BCC charge sets[24] are of comparable quality to HF/6-31G* RESP charge sets,[29] we decided to investigate their suitability for our 3D-QSAR analyses.

Figure 7 shows the variation of the 3D-QSAR cross-validation (LOO) results with the number of PLS components with respect to $q^2$ and the standard error. The CoMFA and CoMSIA results are shown with and without the inclusion of *region focusing*. In the case of CoMSIA, the results are shown with the Gasteiger−Huckel and the AM1-BCC[24] charge sets. As can be seen from Figure 7, the best results are obtained when *region focusing* is included for both CoMFA and CoMSIA, with the

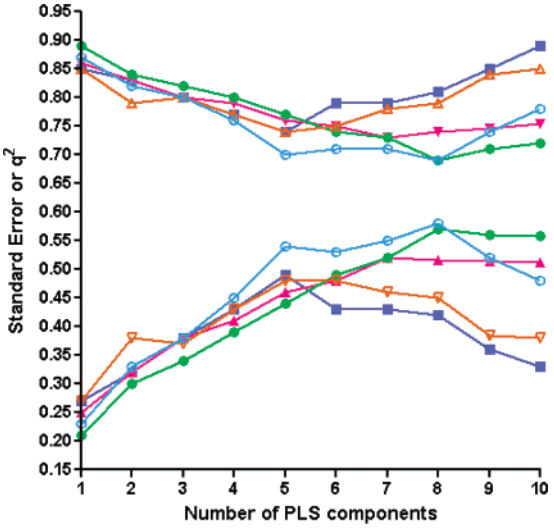


**Figure 7.** Sensitivity of the 3D-QSAR cross-validation results to the charge models and the methodology. The line plots at the top show the standard error as a function of the number of PLS components. The corresponding line plots (with the same color/symbol) at the bottom show $q^2$ (the cross-validated $r^2$) as function of the number of components. The blue squares represent the CoMSIA results with the Gasteiger−Huckel charges; the red solid triangles represent CoMSIA results with the AM1-BCC charge sets; the green solid circles represent the CoMSIA results with *region focusing* and AM1-BCC charge sets; the brown triangles represent the CoMFA results with the AM1-BCC[24] charge sets; and the cyan circles represent CoMFA results with *region focusing*[27] and AM1-BCC charges.

AM1-BCC[24] charge sets for the electrostatic treatment. Additionally, for both the methodologies, the best results are obtained with eight PLS components, with respect to the standard error and $q^2$. When more than eight components are included, both the standard error and $q^2$ declined for the best models (green and cyan). Additional details are given in Tables 8 and 9. For the best models, the fractional electrostatic contribution is larger (at 0.54) for CoMFA, relative to CoMSIA (0.45).

**3D-QSAR Models in Relation to a Proposed Model of the TM3/4 Domain of Rat/Human TRPV1.** In the literature, three different models[2,3,30] were proposed for the capsaicin-binding domain of the TRPV1 channel, which is likely to be the region interacting with TRPV1 inhibitors[20,32] such as those described in this study. Jordt and Julius[2] were the first to suggest an idea for a structural model for the TRPV1 channel. These authors identified the transmembrane helical regions and extracellular loops of the receptor, along with certain critical residues. Though their "model" is basically a schematic idea, it is useful to the biologists for planning/interpreting experiments/results. Gavva et al.[3] performed additional mutation/binding experiments, which implicated additional residues, Thr550 (common to human and rat) and Met547 (in rat TRPV1 but Leu547 in human), and developed their model consistent with these observations and the schematic idea of Jordt and Julius.[2] In the model by Gavva et al.,[3] the vanilloid moiety interacts with Thr550 and the "tail end" hydrophobic group of capsaicin interacts with Tyr511, whereas Jordt and Julius[2] hypothesized that the aromatic portion of Tyr511 interacts with the vanilloid moiety of capsaicin. The model of Middleton and co-workers[30] assumes that vanilloid moiety interacts with Met547, Tyr511, and Tyr555, and their model differs significantly in detail. While the postulated interactions are different in these models, they all agree that the TM3/4 region is the likely vanilloid-binding pocket. Additionally, the capsaicin analogs with changes to the hydroxyl and the methoxy groups that reduce the H-bonding potential display weaker agonist and antagonist activities.[31] It was also shown[20,32] that the TRPV1 antagonists are capsaicin-competitive and some antagonists are able to block all the activation modes of the channel.

The model of TM3 and TM4 proposed by Gavva et al.[3] was based on chimeric and mutagenesis studies on TRPV1, performed after the other two models was published. Vanillyl moiety (methoxy phenol) is common for the TRPV1 agonists, such as capsaicin, RTX, and arvanil, which could interact with the side-chain hydroxyl of Thr550.[3] These studies identified key residues (Met547 and Thr550) in the transmembrane regions 3 and 4 (TM3/4) of rat and human TRPV1 that confer the vanilloid sensitivity and competitive antagonist binding. As the model of Gavva et al.[3] is consistent with these observations, we adopted this structural model for the docking and visualization of some representative cinnamides reported here, with the purpose of showing plausible interactions of the antagonists with the TM3/4 helices, consistent with the 3D-QSAR models proposed here. The model was generated by building the TM3 and TM4 helical protein segments in α-helical conformation, with a loop connecting the helices, using the Biopolymer module of Insight II.[33] This structural model[3] was also employed by Lee et al.[34] for docking and analyzing a different class of the TRPV1 antagonists, similar in size to the current set of ligands. However, this model should be regarded as incomplete (as the structure of the other helices of the receptor are not modeled, which would be significant) and partly speculative until it is confirmed by biophysical studies of the TRPV1 channel.

Figure 8a shows the docked model of **1**, which was obtained by alignment[15] with the docked model of capsaicin,[3] optimized by a protocol recently described.[35] During the optimization of the complex, sidechains of the TM3/4 structural model were relaxed, but the ligand is restrained in its docked, minimum-energy conformation. Based on this optimization, the interactions of this cinnamide with the TRPV1 channel TM3/4 helices were deduced. These include the H-bonding of Arg641 to the carbonyl of the amide, the hydrophobic contacts of the *t*-butyl phenyl and Tyr511, and the interaction of *dihydro benzodioxine* moiety with the side chains of Trp549 and Thr550. These interactions appear to be consistent with the proposed 3D-QSAR models, as shown in Figure 8b. This figure shows the solvent accessible Connolly surface[36] (with a probe radius of 1.4 Å) of our model of the TM3/4 helices color-coded by the molecular lipophilicity potential,[18] calculated from the atomic hydrophobicity scale of Ghose et al.,[37] along with the docked model of **1**. The electrostatic and steric contours from the CoMFA model (the model 3 of Table 8) are also shown superimposed on the surface. Color coding of the Connolly[35] surface by lipophilicity allows clear differentiation of the polar and nonpolar surface regions of the helices and its correspondence to the 3D-QSAR models. It can be seen from Figure 8b that the three green CoMFA contours can be mapped to the van der Waals contacts of the *t*-butyl phenyl moiety with Tyr511 and Arg541. Also, the red CoMFA contour close to the carbonyl oxygen of **1** is proximal to the basic nitrogen of Arg541, consistent with the current structural model. However, due to the incompleteness of the current model and a lack of biophysical characterization of TRPV1 channel, a more elaborate interpretation of the CoMFA contours in terms of the ligand interactions with the channel is not undertaken.

## Conclusion

Two different, predictive 3D-QSAR models (CoMFA and CoMSIA) were developed for the antagonists of TRPV1

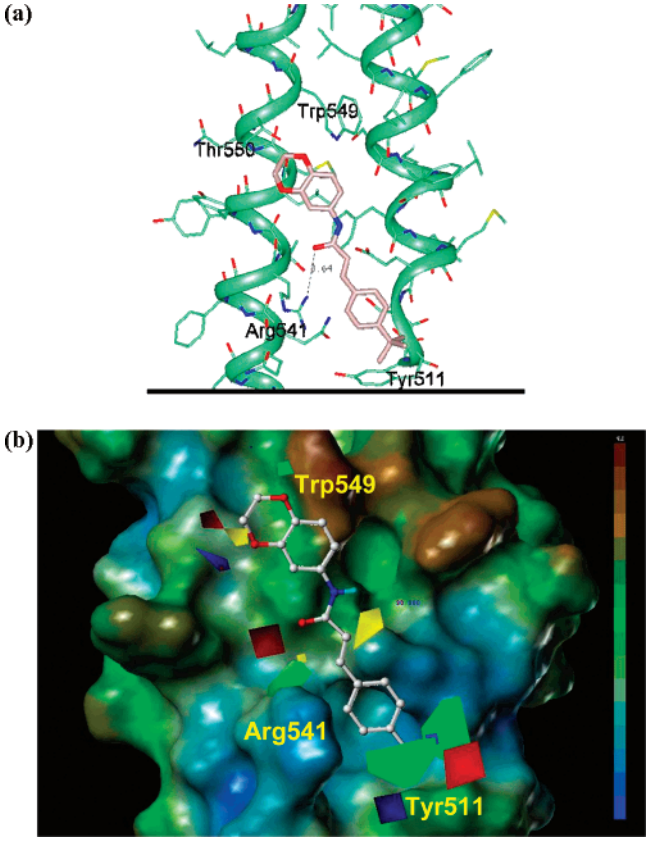


**Figure 8.** (a) Docked model of **1** interacting with TM3 and TM4 of TRPV1. The protein residues likely to contribute significantly to the interactions are identified. The model shows a hydrogen bond between Arg541 side chain and the amide carbonyl of the ligand. The protein model is taken from Gavva et al.[3] (b) Connoly surface[35] of the TM3/4 of TRPV1 channel color-coded by molecular lipophilicity potential[18] (the color scale is shown on right: blue, hydrophilic, to brown, lipophilic). The docked ligand (**1**) is shown along with the CoMFA steric and electrostatic contours (the *steric favored* contour is colored green and the *steric disfavored* contour is colored yellow; the *electropositive favored* contour is colored blue and the *electronegative favored* contour is colored red).

channel, belonging to the cinnamide family. Predictive power for these models was demonstrated for a separate test set of reasonable size. Notably, the training and test sets included 10 or more different substituent positions. Hence, the derived models are quite general and predictive for the cinnamide analogs. It is clearly shown that the use of AM1-BCC[24] charge sets result in much improved correlations and predictions compared to the use of Gasteiger−Huckel[18,23] charge sets, underscoring the importance of the electrostatic treatment. Overall, the statistical results (in terms of $q^2$ and $r^2$) are nearly the same for the CoMFA and CoMSIA models. However, the CoMSIA models offer a better qualitative delineation of structural features contributing to binding affinity and hence are likely to be of greater utility. These models are consistent with a recently proposed model of the TM3/4 helices of the TRPV1 channel, which are shown to be part of the agonist/antagonist binding regions.

**Acknowledgment.** The authors thank Drs. Sung Jin Cho, Michael Bartberger, Narendar Gavva, and Matthew Lee for their helpful comments on the manuscript.

**Supporting Information Available:** Tables of mean, standard deviation, and number of measurements of $IC_{50}$ data for each compound in the training and the test sets. Table of coordinates for the model of TM3/TM4 helices of TRPV1 and the docked structure of **1** (the reference). Figures showing an alignment of the reference in *s-cis*- and *s-trans*-conformations with a conformationally restricted analog. This material is available free of charge via the Internet at http://pubs.acs.org.

## References

(1) Nilius, B.; Voets, T.; Peters, J. TRP channels in disease. *Sci. STKE* **2005**, *2005*, re8, 1−9.
(2) Jordt, S.-E.; Julius, D. Molecular basis for species-specific sensitivity to "hot" chili peppers. *Cell* **2002**, *108*, 421−430.
(3) Gavva, N.; Klionsky, L.; Qu, Y.; Shi, L.; Tamir, R.; Edenson, S.; Zhang, T. J.; Viswanadhan, V. N.; Toth, A.; Pearce, L. V.; Vanderah, T. W.; Porecca, F.; Blumberg, P. M.; Lile, J.; Sun, Y.; Wild, K.; Louis, J.-C.; Treanor, J. J. S. Molecular determinants of vanilloid sensitivity in TRPV1. *J. Biol. Chem.* **2004**, *279*, 20283−20295.
(4) Kwak, J. Y.; Jung, J. Y.; Hwang, S. W.; Lee, W. T.; Oh, U. A capsaicin-receptor antagonist, capsazepine, reduces inflammation-induced hyperalgesic responses in the rat: Evidence for an endogenous capsaicin-like substance. *Neuroscience* **1998**, *86*, 619−626.
(5) Santos, A. R.; Calixto, J. B. Ruthenium red and capsazepine antinociceptive effect in formalin and capsaicin models of pain in mice. *Neurosci. Lett.* **1997**, *235*, 73−76.
(6) Walker, K. M.; Urban, L.; Medhurst, S. J.; Patel, S.; Panesar, M.; Fox, A. J.; McIntyre, P. The VR1 antagonist capsazepine reverses mechanical hyperalgesia in models of inflammatory and neuropathic pain. *J. Pharmacol. Exp. Ther.* **2003**, *304*, 56−62.
(7) Holzer, P. TRPV1 and the gut: From a tasty receptor for a painful vanilloid to a key player in hyperalgesia. *Eur. J. Pharmacol.* **2004**, *500*, 231−241.
(8) Klopman, G.; Li, J. Quantitative structure−agonist activity relationships of capsaicin analogues. *J. Comput.-Aided Mol. Des.* **1995**, *9*, 283−294.
(9) Hosseini, M.; Maddalena, D. J.; Spence, I. Using artificial neural networks to classify the activity of capsaicin and its analogues. *J. Chem. Inf. Comput. Sci.* **1997**, *37*, 1129−1137.
(10) Gunthorpe, M. J.; Rami, H. K.; Jerman, J. C.; Smart, D.; Gill, C. H.; Soffin, E. M.; Hannan, S. L.; Lappin, S. C.; Egerton, J.; Smith, G. D.; Worby, A.; Howett, L.; Owen, D.; Nasir, S.; Davies, C. H.; Thompson, M.; Wyman, P. A.; Randall, A. D.; Davis, J. B. Identification and characterisation of SB-366791, a potent and selective vanilloid receptor (VR1/TRPV1) antagonist. *Neuropharmacology* **2004**, *46*, 133−149.
(11) Doherty, E. M.; Fotsch, C.; Bo, Y.; Chakrabarti, P. P.; Chen, N.; Gavva, N.; Han, N.; Kelly, M. G.; Kincaid, J.; Klionsky, L.; Liu, Q.; Ognayanov, V.; Tamir, R.; Wang, X.; Zhu, J.; Norman, M. H.; Treanor, J. J. S. Discovery of potent, orally available vanilloid receptor-1 antagonists. Structure−activity relationship of *N*-aryl cinnamides. *J. Med. Chem.* **2005**, *48*, 71−90.
(12) Norman, M. H.; Fotsch, C.; Bo, Y.; Chen, N.; Chakrabarthi, P.; Doherty, E. M.; Gavva, N. R.; Nishimura, N.; Nixey, T.; Ognayanov, V. I.; Rzasa, R. M.; Stec, M.; Surapaneni, S.; Tamir, R.; Viswanadhan, V. N.; Treanor, J. J. S. Novel vanilloid receptor-1 antagonists: 1. Conformationally restricted analogues of *trans*-cinnamides. *J. Med. Chem.* **2007**, *50*, 3497−3514.
(13) Cramer, R. D., III; Patterson, D. E.; Bunce, J. E. Comparative molecular field analysis (CoMFA). 1. Effect of shape on binding of steroids to carrier proteins. *J. Am. Chem. Soc.* **1988**, *110*, 5959−5967.
(14) Klebe, G.; Abraham, U.; Mietzner, T. Molecular similarity indices in a comparative analysis (CoMSIA) of drug molecules to correlate and predict their biological activity. *J. Med. Chem.* **1994**, *37*, 4130−4146.
(15) Cho, S.-J.; Sun, Y. FLAME: A program to flexibly align molecules. *J. Inf. Model.* **2006**, *46*, 298−306. FLAME is implemented as a C++ program, using OpenEye toolkits, OEChem and CASE, available at http://www.eyesopen.com.
(16) Halgren, T. A. MMFF forcefield. *J. Comput. Chem.* **1996**, *17*, 490−519.
(17) Still, W. C.; Tempczyk.; A.; Hawley, R. C.; Hendrickson, T. Semianalytic treatment of solvation for molecular mechanics and dynamics. *J. Am. Chem. Soc.* **1990**, *112*, 6127−6129.
(18) Tripos Associates, Inc. *Sybyl*, 7.1 ed.; St. Louis, MO.
(19) Frisch, M. J.; Trucks, G. W.; Schlegel, H. B.; Scuseria, G. E.; Robb, M. A.; Cheeseman, J. R.; Zakrzewski, V. G.; Montgomery, J. A., Jr.; Stratmann, R. E.; Burant, J. C.; Dapprich, S.; Millam, J. M.; Daniels, A. D.; Kudin, K. N.; Strain, M. C.; Farkas, O.; Tomasi, J.; Barone, V.; Cossi, M.; Cammi, R.; Mennucci, B.; Pomelli, C.; Adamo, C.; Clifford, S.; Ochterski, J.; Petersson, G. A.; Ayala, P. Y.; Cui, Q.; Morokuma, K.; Malick, D. K.; Rabuck, A. D.; Raghavachari, K.; Foresman, J. B.; Cioslowski, J.; Ortiz,

J. V.; Stefanov, B. B.; Liu, G.; Liashenko, A.; Piskorz, P.; Komaromi, I.; Gomperts, R.; Martin, R. L.; Fox, D. J.; Keith, T.; Al-Laham, M. A.; Peng, C. Y.; Nanayakkara, A.; Gonzalez, C.; Challacombe, M.; Gill, P. M. W.; Johnson, B. G.; Chen, W.; Wong, M. W.; Andres, J. L.; Head-Gordon, M.; Replogle, E. S.; Pople, J. A. *Gaussian 98*, revision A.11.3; Gaussian, Inc.: Pittsburgh, PA, 1998.

(20) Gavva, N.; Tamir, R.; Qu, Y.; Klionsky, L.; Zhang, T. J.; Immke, D.; Wang, J.; Zhu, D.; Vanderah, T. W.; Prreca, F.; Doherty, E. M.; Norman, M. H.; Wild, K. D.; Bannon, A. W.; Louis, J.-C.; Treanor, J. J. S. AMG 9810 [(*E*)-3-(4-*t*-butylphenyl)-*N*-(2,3-dihydrobenzo[*b*]-[1,4]dioxin-6-yl)acrylamide], a novel vanilloid receptor 1 (TRPV1) antagonist with antihyperalgesic properties. *J. Pharm. Exp. Ther.* **2005**, *313*, 474−484.

(21) Pearlman, R. S. Rapid generation of high quality approximate 3D molecular structures. *Chem. Des. Aut. News* **1987**, *1*, 5−7.

(22) Rusinko, A., III.; Skell, J. M.; Balducci, R.; Pearlman, R. S. *A Program for the rapid generation of high quality approximate 3-dimensional molecular structures*; Abstracts of 192nd American Chemical Society Meeting, Anaheim, CA, 1986; CONCORD is distributed by Tripos International, St. Louis, MO 63144, U.S.A.; www.tripos.com.

(23) Gasteiger, J.; Marsili, M. Iterative partial equalization of orbital electronegativity−A rapid access to atomic charges. *Tetrahedron* **1980**, *36*, 3219−3228.

(24) Jakalian, A.; Bush, B. L.; Jack, D. B.; Bayly, C. I. Fast, efficient generation of high-quality atomic charges. AM1-BCC model: I. Method. *J. Comput. Chem.* **2000**, *21*, 132−146.

(25) Viswanadhan, V. N.; Ghose, A. K.; Revankar, G. R.; Robins, R. K. Atomic physico-chemical properties for three dimensional quantitative structure-activity relationships. IV. Additional parameters for hydrophobic and dispersive interactions and their appplication for the superposition of certain naturally occurring antibiotics. *J. Chem. Inf. Comput. Sci.* **1989**, *29*, 163−172.

(26) Bush, B. L.; Nachbar, J., R. B. Sample-distance partial least squares: PLS optimized for many variables. *J. Comput.-Aided Mol. Des.* **1993**, *7*, 587−619.

(27) Cho, S. J; Tropsha, A. Cross-validated R2-guided region selection for comparative molecular field analysis: A simple method to achieve consistent results. *J. Med. Chem.* **1995**, *38*, 1060−1066.

(28) Jayatilleka, P. R. N.; Nair, A. C.; Zauhar, R.; Welsh, W. J. HIV-1 protease inhibitors: Influence of calculated inhibitor-enzyme binding affinities on the statistical quality of 3D-QSAR CoMFA models. *J. Med. Chem.* **2000**, *43*, 4446−2251.

(29) Bayly, C. I.; Cieplak, P.; Cornell, W. D.; Kollman, P. A. A well-behaved electrostatic potential based method using charge restraints for deriving atomic charges: The RESP model. *J. Phys. Chem.* **1993**, *97*, 10269−10280.

(30) Chou, M. Z.; Mtui, T.; Gao, Y.-D.; Kohler, M.; Middleton, R. E. Resiniferatoxin binds to the capsaicin receptor (TRPV1) near extracellular side of the S4 transmembrane domain. *Biochemistry* **2004**, *43*, 2501−2511.

(31) Walpole, C. S.; Wrigglesworth, R.; Bevan, S.; Campbell, E. A.; Dray, A.; James, I. F.; Perkins, M. N.; Reid, D. J.; Winter, J. Analogues of capsaicin with agonist activity as novel analgesic agents: Structure−activity studies. 1. The aromatic "A-region". *J. Med. Chem.* **1993**, *36*, 2362−2372.

(32) Gavva, N. R.; Tamir, R.; Klinosky, L.; Norman, M. H.; Louis, J.-C.; Wild, K.; Treanor, J. J. S. Proton activation does not alter antagonist interaction with the capsaicin-binding pocket of TRPV1. *J. Med. Chem.* **2005**, *68*, 1524−1533.

(33) Lee, J.; Jin, M.-K.; Kang, S.-U.; Kim, S. Y.; Lee, J.; Shin, M.; Hwang, J.; Cho, S.; Choi, Y.-S.; Choi, H.-K.; Kim, S.-E.; Suh, Y.-G.; Lee, Y.-S.; Kim, Y.-H.; Ha, H.-J.; Toth, A.; Pearce, L. V.; Tran, R.; Szabo, T.; Welter, J. D.; Lundberg, D. J.; Wang, Y.; Lazar, J.; Pavlyukovets, V. A.; Morgan, M. A.; Blumberg, P. M. Analysis of structure−activity relationships for the "B-region" of *N*-(4-*t*-butylbenzyl)-*N*′-[4-(methylsulfonylamino)benzyl]-thiourea analogues as TRPV1 antagonists. *Bioorg. Med. Chem. Lett.* **2005**, 4143−4150

(34) *Insight II*; Accelrys, Inc.: San Diego, CA (www.accelrys.com).

(35) Lee, M.; Sun, Y. Improving docking accuracy through molecular mechanics generalized Born optimization and scoring. *J. Chem. Theory Comput.* **2007**, *3*, 1106−1119.

(36) Connolly, M. L. Solvent accessible surfaces of proteins and nucleic acids. *Science* **1983**, *221*, 709−713.

(37) Ghose, A. K.; Viswanadhan, V. N.; Wendoloski, J. J. Prediction of hydrophobic (lipophilic) properties of small organic molecules using fragmental methods: An analysis of ALOGP and CLOGP methods. *J. Phys. Chem. A* **1998**, *102*, 3762−3772.

JM070261K